Changing Morphology of BaO/Al_2O_3 during NO_2 Uptake and Release

János Szanyi,*,† Ja Hun Kwak,† Jonathan Hanson,‡ Chongmin Wang,†,§ Tamás Szailer,† Charles H. F. Peden†

Interfacial Chemistry and Engineering, Chemical Sciences Division and Environmental Molecular Sciences Laboratory, Pacific Northwest National Laboratory, P.O. Box 999, MSIN: K8-93, Richland, Washington 99352, and Department of Chemistry, Brookhaven National Laboratory, Upton, New York 11973

Received: December 22, 2004; In Final Form: February 4, 2005

The changes in the morphology of Ba-oxide-based NO_x storage/reduction catalysts were investigated using time-resolved X-ray diffraction, transmission electron microscopy, and energy dispersed spectroscopy. Large $Ba(NO_3)_2$ crystallites form on the alumina support when the catalyst is prepared by the incipient wetness method using an aqueous $Ba(NO_3)_2$ solution. Heating the sample to 873 K in a He flow results in the decomposition of the $Ba(NO_3)_2$ phase and the formation of both a monolayer BaO film strongly interacting with the alumina support and nanocrystalline BaO particles. Upon NO_2 exposure of these BaO phases at room temperature, small (nanosized) $Ba(NO_3)_2$ crystals and a monolayer of surface nitrate form. Heating this sample in NO_2 results in the coalescence of the nanocrystalline $Ba(NO_3)_2$ particles into large crystals. The average crystal size in the reformed $Ba(NO_3)_2$ layer is significantly smaller than that measured after the catalyst preparation. Evidence is also presented for the existence of a monolayer $Ba(NO_3)_2$ phase after thermal treatment in NO_2, in addition to these large crystals. These results clearly demonstrate the dynamic nature of the Ba-containing phases that are active in the NO_x storage/reduction process. The proposed morphology cycle may contribute to the understanding of the changes observed in the performances of these catalysts during actual operating conditions.

Introduction

One of the key challenges facing the catalysis community is the elimination of harmful gases emitted by internal combustion engines. In particular, the reduction of NO_x from an exhaust gas mixture that contains an excess amount of oxygen is difficult. Traditional three-way catalysts do not work under lean conditions because the concentrations of the reductants (CO and hydrocarbons) are greatly reduced by their oxidation with O_2 on the noble metal components of these catalysts. Therefore, new approaches to NO_x reduction have been considered in the past decade. Despite all the efforts to develop new emission control technologies for lean NO_x reduction, only limited applications have been achieved. One of the most promising technologies under consideration is the NO_x storage/reduction (NSR) method. This process is based on the ability of certain oxides, in particular, alkaline and alkaline earth oxide materials, to store NO_x under lean conditions and to release it during rich (excess reductant) engine operation cycles. Since the original reports on this technology from Toyota in the mid 1990s,[1,2] several research groups have focused on understanding both the NO_x adsorption and the reduction cycles.[3−18] The most extensively studied catalyst systems are based on BaO supported by Al_2O_3. Vibrational spectroscopy and temperature programmed desorption are commonly used to identify the nature and stabilities of NO_x species formed in the uptake cycle.[3−5,7,9,13−19] During NO_x uptake, the $BaO/BaCO_3$ phase is converted to $Ba(NO_3)_2$ that, in turn, releases NO_x in the rich cycle and reforms the active NO_x storage phase of BaO. Also in this latter cycle, the released NO_x is reduced by hydrocarbons and CO on the noble metal components of the fully formulated catalyst, similar to three-way catalysis. The results of our combined IR, TPD, and ^{15}N solid-state NMR study[19] suggested that, upon NO_2 adsorption, there are changes in the morphology of the BaO/Al_2O_3 catalysts. We proposed the formation of a monolayer Ba-nitrate film on the support upon elevated temperature NO_2 adsorption and the formation of large $Ba(NO_3)_2$ crystals. The ratio of NO_x stored in the interfacial monolayer Ba-nitrate to that stored as bulk nitrate varies with BaO coverage. The mobility of the active BaO phase on the alumina support has been suggested[18] and was proposed to be one of the reasons for the deactivation of the catalyst in repeated cycles. The continuously changing dynamic surface may promote both the aggregation of Pt particles and the formation of a Ba-containing layer on the Pt particles. Both of these processes may eventually lead to catalyst deactivation.

In this work, we focused on the changes in the morphology of the active Ba-containing phase during thermal decomposition and NO_2 uptake using time-resolved X-ray diffraction (TR-XRD) and transmission electron microscopy/energy dispersive X-ray spectroscopy (TEM/EDS) techniques.

Experimental Procedures

The 20 wt % BaO/Al_2O_3 catalyst was prepared by the incipient wetness method using an aqueous $Ba(NO_3)_2$ solution. The γ-alumina (Aldrich) used as the support for catalyst preparation had a surface area of 200 m^2/g. Decomposition of the formed $Ba(NO_3)_2$ on Al_2O_3 was studied in time-resolved X-ray diffraction (TR-XRD). The TR-XRD experiments were

* Corresponding author. E-mail: janos.szanyi@pnl.gov.
† Chemical Sciences Division.
‡ Brookhaven National Laboratory.
§ Environmental Molecular Sciences Laboratory.

10.1021/jp044160z CCC: $30.25
Published on Web 03/17/2005

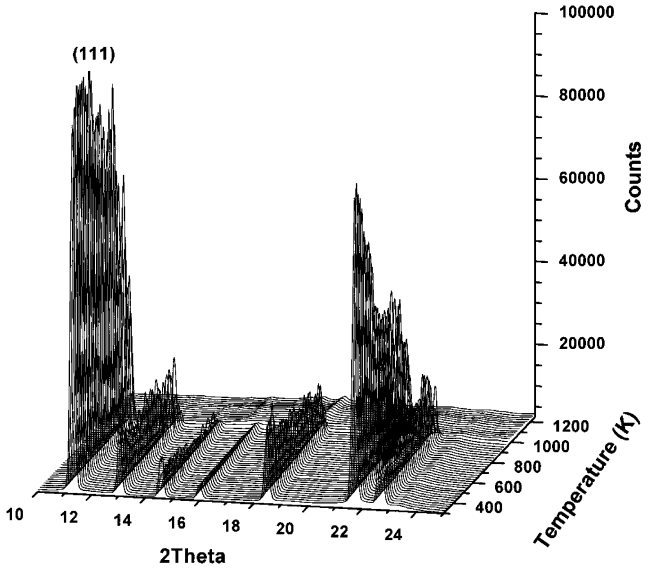

Figure 1. TR-XRD patterns collected during temperature programmed decomposition from an as-prepared $Ba(NO_3)_2/Al_2O_3$ sample.

carried out at beam line X7B of the National Synchrotron Light Source (NSLS), at Brookhaven National Laboratory. The detailed experimental setup has been discussed elsewhere.[20] In the decomposition experiments, a small amount of $Ba(NO_3)_2/Al_2O_3$ sample was heated at a constant rate from 300 to 1250 K. XRD patterns were collected during the NO_2 adsorption experiments at 300 K and in temperature programmed experiments in which the sample was exposed to a constant NO_2 flow while heated from 300 to 573 K (in the NO_2 uptake experiments. a 250 ppm NO_2/He gas mixture was used). Prior to these experiments, the catalyst was calcined at 873 K to ensure the formation of BaO/Al_2O_3. After the completion of the NO_2 adsorption at 573 K, the sample was cooled to 300 K in flowing NO_2, purged with He, and then heated in He flow to 873 K to induce the decomposition of the NO_x species formed during NO_2 uptake.

TEM images were collected from the alumina support, the as-prepared $Ba(NO_3)_2$ on Al_2O_3, BaO/Al_2O_3, and high-temperature (673 K) NO_2-exposed BaO/Al_2O_3 samples. TEM specimens were prepared by dusting the powder particles onto a carbon film coated 200 mesh copper TEM grid. High-resolution TEM analysis was carried out on a JEOL JEM 2010 microscope with a specified point-to-point resolution of 0.194 nm. The operating voltage on the microscope was 200 keV. All images were digitally recorded with a slow scan CCD camera (image size 1024 × 1024 pixels), and image processing was carried out using a Digital Micrograph (Gatan). The composition of the particles was analyzed by energy-dispersive X-ray spectroscopy (EDS). The spectrometer is Oxford Link system and is attached onto the transmission electron microscope.

Results and Discussion

A series of XRD patterns obtained during temperature programmed decomposition of the as-prepared $Ba(NO_3)_2/Al_2O_3$ in a He flow is shown in Figure 1 in the 300−1255 K temperature range. The room-temperature XRD pattern of the as-prepared and dried material contains peaks that can be assigned to crystalline $Ba(NO_3)_2$ and γ-alumina. Up to about 650 K, the characteristic diffraction peaks are practically unchanged, suggesting that the $Ba(NO_3)_2$ crystallites are stable on the alumina surface in the 300−650 K temperature range. Heating the sample above 650 K results in a rapid decrease in

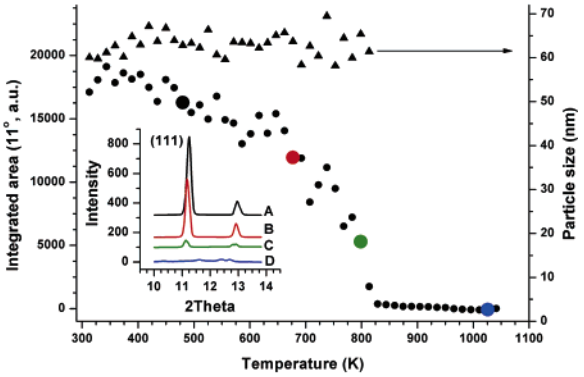

Figure 2. Integrated area of the (111) diffraction peak (at $2\theta = 11.6°$) and the average particle size of $Ba(NO_3)_2$ crystallites as a function of sample temperature (results extracted from the patterns of Figure 1). The inset shows XRD patterns at selected sample temperatures: A, 473 K; B, 673 K; C, 800 K; and D, 1025 K.

the intensities of all $Ba(NO_3)_2$-related diffraction features. The variation of the integrated intensity of the (111) diffraction feature with increasing sample temperature is displayed in Figure 2. The inset in this figure shows selected XRD patterns collected at 473, 673, 800, and 1025 K sample temperatures. The results shown in these figures clearly indicate the complete decomposition of $Ba(NO_3)_2$ on the alumina surface by the time the sample temperature reaches 823 K, more than 100 K lower than that reported for the decomposition of unsupported $Ba(NO_3)_2$ (>920 K). These results are in agreement with our previously reported data[19] in which we have shown that, due—most probably—to a strong oxide−oxide interaction, the $Ba(NO_3)_2$ phase that formed upon NO_2 uptake decomposed at much lower temperature than the unsupported bulk $Ba(NO_3)_2$. This figure also displays the average particle size—as calculated from the fwhm of the (111) diffraction peak—as a function of sample temperature. Interestingly, the average particle size of about 60 nm does not change with sample temperature up to the point where the nitrate phase completely disappears. After the decomposition of the $Ba(NO_3)_2$ phase, only the strong diffraction features of the alumina support and the very weak intensity, broad peaks of nanocrystalline BaO can be seen. Increasing the sample temperature above 1000 K results in the formation of a $BaAl_2O_4$ phase, and its characteristic diffraction features gradually develop in the XRD patterns as the broad features of the nanosized BaO crystallites disappear.

The effect of NO_2 uptake on the morphology of the Ba-containing active phase was investigated next. Prior to NO_2 uptake, the as-prepared $Ba(NO_3)_2/Al_2O_3$ sample was calcined in flowing oxygen at 773 K for 2 h to form a 20 wt % BaO/Al_2O_3 material. In the XRD pattern obtained from this sample, we did not observe any traces of the Ba-nitrate phase. The only diffraction features seen after the annealing cycle are the strong peaks of γ-alumina, very broad peaks of BaO, and some characteristic peaks of $Ba(CO_3)_2$ (JCPDS 05-0378). A small amount of $Ba(CO_3)_2$ was formed after the exposure of the activated catalyst to an atmosphere that contained CO_2 and H_2O. (The calcination temperature of 773 K is insufficiently high to have all the carbonate phase decomposed. However, the presence of this minority carbonate phase does not influence the interpretation of our results.) The very broad XRD features of BaO indicate the formation of nanosized particles as $Ba(NO_3)_2$ decomposes. When this sample is exposed to a gas stream containing 250 ppm NO_2 in He at 300 K, the formation of a nanocrytalline $Ba(NO_3)_2$ phase is observed as evidenced by the development of broad diffraction features in the XRD patterns. A series of XRD patterns recorded during the NO_2

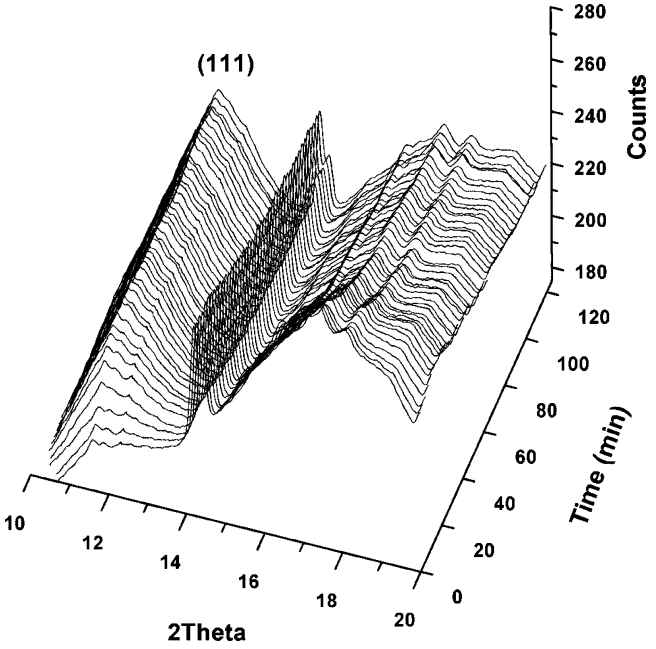

Figure 3. XRD patterns collected during NO_2 exposure of the 20 wt % BaO/Al_2O_3 sample at room temperature for 2 h.

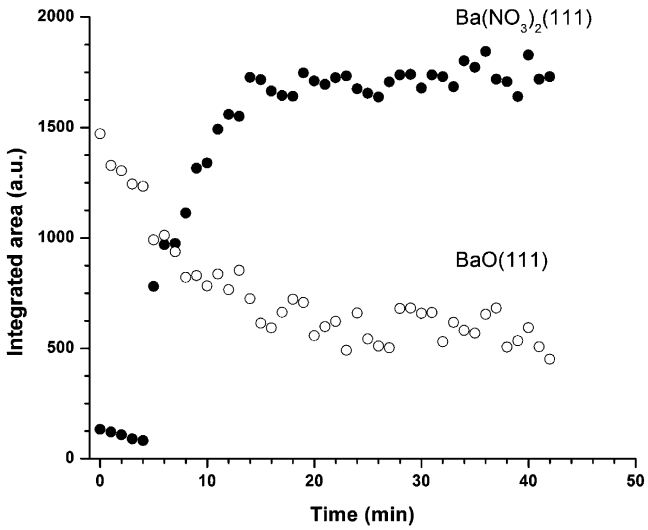

Figure 4. Integrated intensities of the (111) X-ray diffraction features of BaO and $Ba(NO_3)_2$ as a function of NO_2 exposure time at 300 K. Catalyst: 20 wt % BaO/Al_2O_3.

uptake at 300 K is shown in Figure 3 as a function of exposure time. These nanocrystalline $Ba(NO_3)_2$ particles formed in the reaction of BaO nanocrystals with NO_2. It is noteworthy that no $Ba(NO_2)_2$ phase is seen at all at the beginning of NO_2 exposure of the BaO phase. Vibrational spectroscopic studies[13−19] suggested that $Ba(NO_2)_2$ forms first and then it is converted to $Ba(NO_3)_2$ by the excess NO_2 present. The XRD pattern recorded after NO_2 exposure of the BaO/Al_2O_3 sample clearly matches JCPDS pattern 24-0053 and the one calculated by Nowotny et al. for single crystalline $Ba(NO_3)_2$.[21] On the other hand, it does not have any correspondence with JCPDS 36-0449 or the calculated pattern from single crystalline $Ba(NO_2)_2$.[22] The integrated intensity of the (111) diffraction feature of the formed $Ba(NO_3)_2$ together with that of the (111) diffraction peak of the nanocrystalline BaO are displayed in Figure 4 as a function of time the sample is exposed to NO_2 (first 42 min of exposure). The results shown in this figure clearly demonstrate that the intensity of the (111) diffraction feature of BaO nanoparticles

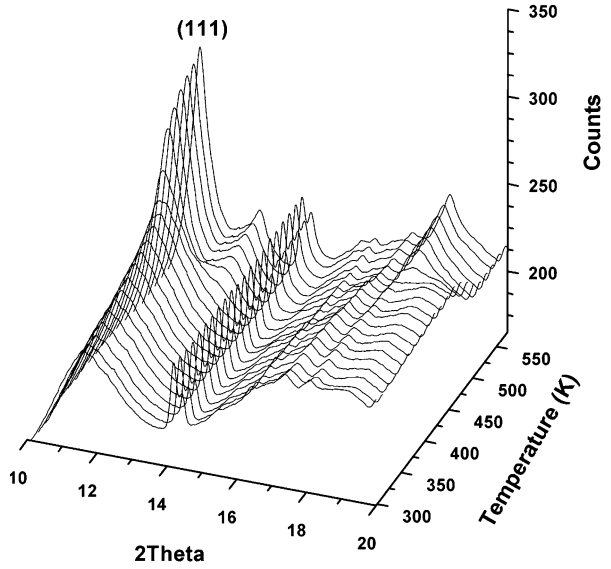

Figure 5. XRD patterns recorded from a 20 wt % BaO/Al_2O_3 sample upon NO_2 exposure in the 300−573 K temperature range.

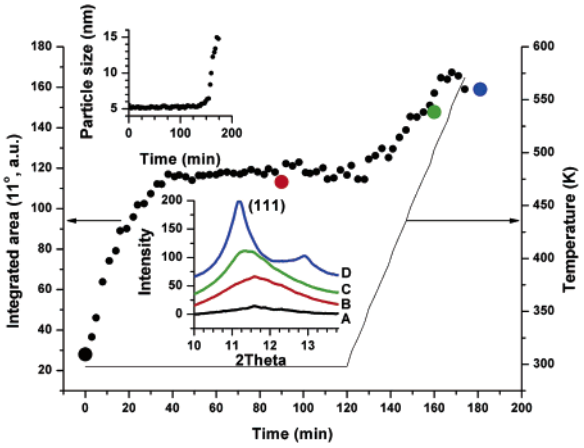

Figure 6. Integrated intensity of the (111) diffraction feature of $Ba(NO_3)_2$ particles during exposure of a 20 wt % BaO/Al_2O_3 sample to NO_2 at room temperature and in the 300−573 K temperature range (results extracted from the XRD patterns of Figures 4 and 5). [In the inset, the XRD pattern A was collected at $t = 0$ at 300 K, B at $t = 90$ min at 300 K, C at 573 K, and D at 673 K.]

decreases while that of the $Ba(NO_3)_2$ phase increases. After exposing the sample to NO_2 at room temperature for 2 h, the temperature was raised to 573 K, and changes in the XRD patterns were monitored as a function of sample temperature under flowing NO_2. The diffraction features characteristic of crystalline $Ba(NO_3)_2$ became sharper and more intense as the temperature was raised from 300 to 573 K (Figure 5). In Figure 6, the changes in the integrated peak intensity of the (111) diffraction feature, and the average $Ba(NO_3)_2$ particle size (in the inset) estimated from the fwhm of the (111) peak during both room temperature and elevated temperature NO_2 uptake, are displayed. The integrated intensities of the $Ba(NO_3)_2$-related diffraction peaks increase in the first 40 min of NO_2 exposure at 300 K and stay constant for an additional 2 h of NO_2 exposure. In this time interval, the average particle size remains unchanged at about 5 nm. Changes in both the integrated peak intensities and the average particle size occur as the sample is heated from 300 to 573 K. The integrated intensity of the (111) diffraction peak increases about 30% in this temperature range, while the average particle size increases from 5 to 15 nm. These results indicate that, at room temperature, the conversion of the

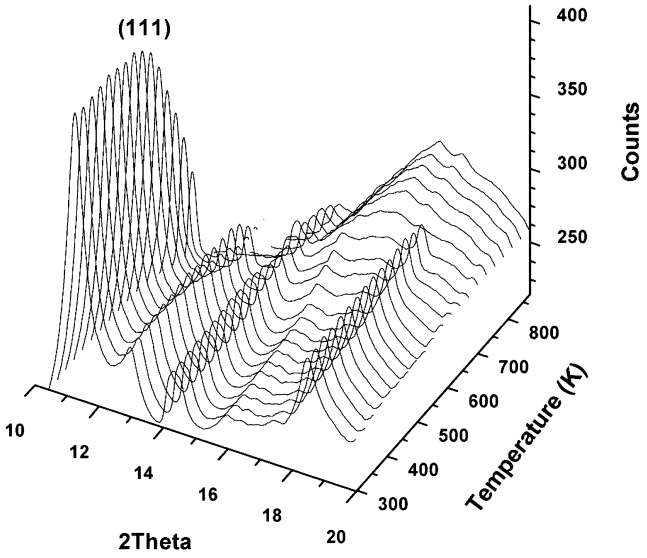

Figure 7. TR-XRD patterns collected during the decomposition of $Ba(NO_3)_2$ in a He flow following NO_2 uptake at 573 K.

nanosized BaO particles into $Ba(NO_3)_2$ nanocrystals is fast and that the mobility of the formed $Ba(NO_3)_2$ crystallites increases dramatically with temperature. Above 340 K, the particle size increases rapidly and in an approximately linear fashion with sample temperature. XRD patterns collected at selected temperatures in the inset of Figure 6 show that the initially very broad (111) XRD feature actually contains two very broad, low intensity features (due to the overlapping of the (111) and (200) diffraction traces). The overlap of these two diffraction features at the beginning of NO_2 uptake may result in an underestimation of the average particle size at low NO_2 levels. As larger $Ba(NO_3)_2$ crystallites form, these two diffraction peaks are sharp and well-separated. The $Ba(NO_3)_2$ crystallites formed in the high-temperature NO_2 uptake have a much smaller average particle size (15 nm) than the $Ba(NO_3)_2$ particles formed during catalyst preparation from an aqueous $Ba(NO_3)_2$ solution (~60 nm). No change in the XRD pattern is seen while cooling the sample to room temperature following the high-temperature NO_2 uptake.

Changes in the XRD pattern upon temperature programmed decomposition of the $Ba(NO_3)_2$ phase following NO_2 uptake at 573 K are displayed in Figure 7. The diffraction features characteristic of crystalline $Ba(NO_3)_2$ are stable up to around 573 K, then their intensities decrease significantly as the temperature is raised to ~673 K, and at even higher temperatures, they completely disappear. The changes in the integrated intensity of the (111) diffraction peak as a function of temperature are displayed in Figure 8. The inset in this figure shows that the average particle size of the $Ba(NO_3)_2$ crystallites stays constant at around 17 nm up to ~560 K. As the temperature is raised further, the integrated intensity of the (111) diffraction peak (and all the other $Ba(NO_3)_2$-related features) decreases, while the average particle size increases. At ~700 K, the average particle size nearly doubles in comparison to that bellow 560 K (~32 vs 17 nm). This suggests that as $Ba(NO_3)_2$ starts decomposing above 573 K and the BaO film forms on the alumina support,[19] the remaining crystallites agglomerate to form larger particles. One might suggest that the $Ba(NO_3)_2$ phase melts and decomposes. However, this is highly unlikely since the melting point of $Ba(NO_3)_2$ (850 K) is significantly higher than the temperature where the decomposition of the $Ba(NO_3)_2$ crystallites was observed. At temperatures above 700 K, these large crystals decompose as well, resulting in the reformation

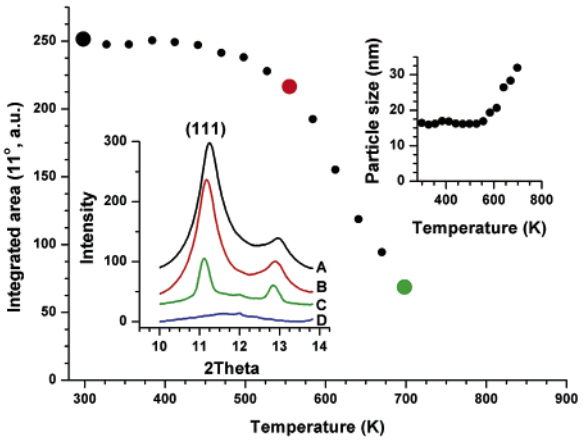

Figure 8. Changes in the integrated intensity of the (111) diffraction feature as a function of sample temperature (results extracted from the diffraction patterns of Figure 6). The insets show the changes in the average particle size as a function of temperature and also XRD patterns at selected sample temperatures.

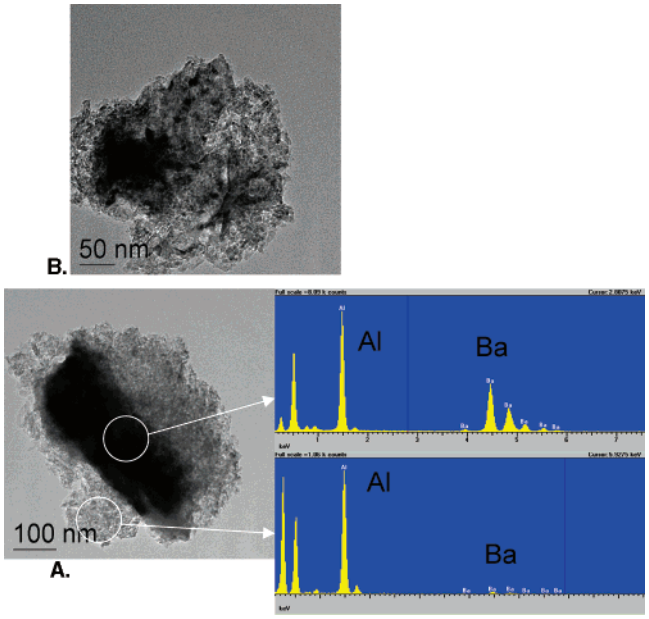

Figure 9. TEM images from the as-prepared $Ba(NO_3)_2/Al_2O_3$ sample (the precursor for the 20 wt % BaO/Al_2O_3 material). EDS spectra from two selected spots showing the very different compositions in these two regions of the sample. (A: a very large (the largest we could find) $Ba(NO_3)_2$ crystallite on the Al_2O_3 support and B: a representative image of the $Ba(NO_3)_2/Al_2O_3$ system.)

of alumina-supported BaO nanoparticles. In the diffraction patterns of Figure 7 above 700 K, all the representative Ba-nitrate features are absent, and only the very broad diffraction feature of the nanosized BaO phase is present.

The changing morphology of the BaO/Al_2O_3 system upon NO_2 uptake and release was also investigated by TEM. Information about the surface composition was obtained using EDS. TEM images from an as-prepared $Ba(NO_3)_2/Al_2O_3$ sample are shown in Figure 9. In panel A**,** a large $Ba(NO_3)_2$ crystal can be seen on the alumina support (in fact, this was the largest crystallite we found on this material). The size of the $Ba(NO_3)_2$ crystal is about 300 nm × 150 nm. EDS results for two selected regions of this catalyst particle are also shown as an inset. EDS analysis confirms that the large, dark-shaded crystal seen in the TEM image is $Ba(NO_3)_2$, while there is no $Ba(NO_3)_2$ dispersed on the alumina support. Panel B of Figure 9 shows a more characteristic image of the $Ba(NO_3)_2/Al_2O_3$ sample, with

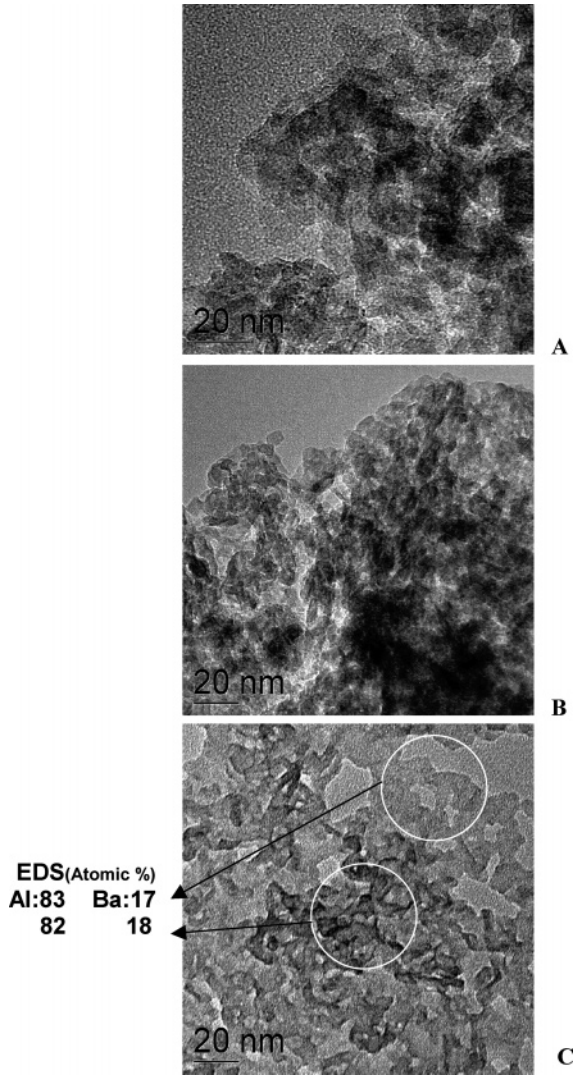

Figure 10. TEM images from Al_2O_3 (A), 8 wt % (B), and 20 wt % BaO/Al_2O_3 (C) samples. The results of EDS analysis are also shown for two selected spots on the 20 wt % BaO/Al_2O_3 sample.

$Ba(NO_3)_2$ particle sizes in the 50−70 nm range, in agreement with the results of the XRD analysis discussed previously (most of the $Ba(NO_3)_2$ crytallites observed in all the TEM images of this sample fell in this size range). In summary, we can conclude that large $Ba(NO_3)_2$ crystals (from tens of nanometers to hundreds of nanometers in size) form on the alumina support upon the incipient wetness catalyst preparation with an aqueous $Ba(NO_3)_2$ solution. A small fraction of the alumina surface is covered by these $Ba(NO_3)_2$ crystals, while most of the support is Ba-free.

We have already shown that heating an as-prepared and dried $Ba(NO_3)_2/Al_2O_3$ catalyst at 773 K in flowing air resulted in the decomposition of $Ba(NO_3)_2$ crystallites and the formation of nanosized BaO particles on the alumina support. The morphology of the resulting catalyst closely resembles that of the alumina support. TEM images, collected with the same resolution, of the Al_2O_3 support and 773 K calcined 8 and 20 wt % BaO/Al_2O_3 materials are displayed in Figure 10. The TEM images of both BaO-containing samples are very similar to that of the alumina support. EDS analysis of the 20 wt % BaO/Al_2O_3 catalyst confirms the even distribution of the Ba-containing phase on the alumina support. The two spots analyzed (a light and a dark spot in TEM in Figure 10) show practically the same Al/Ba atomic ratios (83:17 and 82:18, respectively).

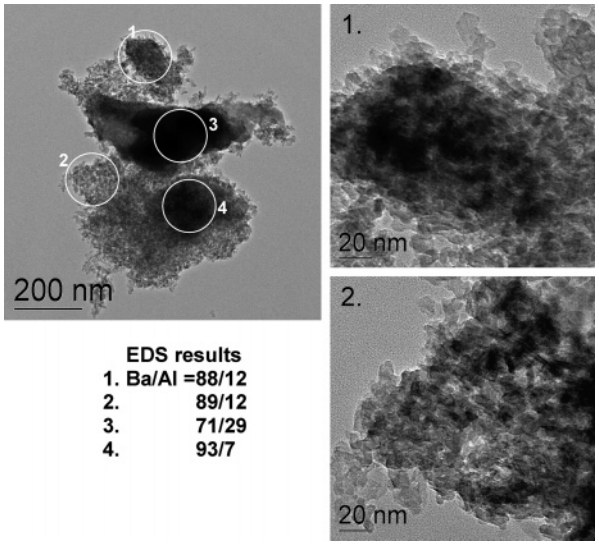

Figure 11. TEM images obtained following NO_2 uptake at 573 K on the 20 wt % BaO/Al_2O_3 sample. EDS results from selected spots on this sample are also displayed. High-resolution TEM images of spots 1 and 2 are also displayed.

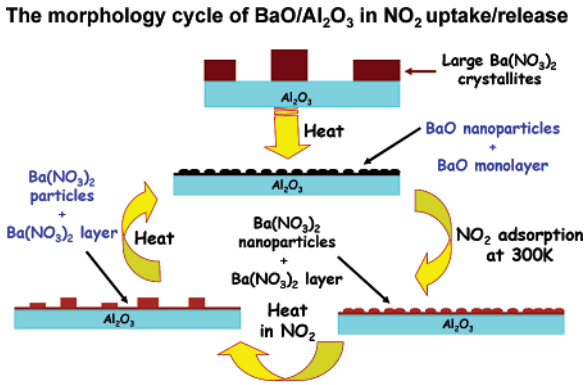

Figure 12. Schematics of the cycle of morphology changes taking place during NO_2 uptake and release on BaO/Al_2O_3 NO_x storage/reduction materials.

TEM images from a 20 wt % BaO/Al_2O_3 sample after saturation with NO_2 at 573 K are displayed in Figure 11. The formation of $Ba(NO_3)_2$ crystals during NO_2 uptake is evidenced by the appearance of dark spots in the TEM images. This process is further substantiated by the results of EDS analysis on selected spots of this sample. It is interesting to note that we detected Ba everywhere on the sample, not just at the places where the presence of $Ba(NO_3)_2$ crystallites are evident from the TEM images. These findings suggest that the material formed during the uptake of NO_2 has a different morphology and spatial composition than the starting material prepared by the incipient wetness method. In the former case, we observe Ba-containing material all over the alumina surface, together with large $Ba(NO_3)_2$ crystallites. These crystallites, however, are smaller in size than those formed in the incipient wetness procedure.

The proposed cycle of morphology changes for a BaO/Al_2O_3 NSR catalyst is summarized in the scheme of Figure 12. The as-prepared $Ba(NO_3)_2/Al_2O_3$ material consists of large (>60 nm) $Ba(NO_3)_2$ crystallites positioned on the Al_2O_3 support. Most of the support surface is Ba-free. Heating this material to temperatures above 800 K results in the complete decomposition of the $Ba(NO_3)_2$ phase and the formation of a thin layer of BaO and BaO nanoparticles on top of this layer. The thus formed BaO/Al_2O_3 catalyst adsorbs NO_2 at 300 K without changing the morphology of the system (i.e., small, nanosized $Ba(NO_3)_2$

crystallites form). Conducting the NO_2 uptake at a higher temperature (573 K) results in the agglomeration of the small $Ba(NO_3)_2$ crystallites with an average particle size of ~15 nm. In the resulting $Ba(NO_3)_2/Al_2O_3$ system, the average $Ba(NO_3)_2$ particle size is about 25% of that seen in the as-prepared $Ba(NO_3)_2/Al_2O_3$ material. Also, in the $Ba(NO_3)_2/Al_2O_3$ system we obtained during the NO_2 uptake, we can detect Ba all over the alumina support, while in the as-prepared one there was only a fraction of the alumina support surface that was actually covered with $Ba(NO_3)_2$ crystals. Thus, the thin BaO (monolayer) film adsorbs NO_2 as well, forming a stable $Ba(NO_3)_2$ monolayer in addition to $Ba(NO_3)_2$ particles as depicted at the bottom of Figure 12.

The formation of this thin $Ba(NO_3)_2$ layer (monolayer) is probably responsible for the low-temperature NO_2 desorption feature we have observed in our temperature programmed decomposition study.[19] After the decomposition of this thin $Ba(NO_3)_2$ layer to reform a thin BaO film, the remaining $Ba(NO_3)_2$ particulate phase decomposes in the same way as unsupported, bulk $Ba(NO_3)_2$ does (i.e., by releasing $2NO + 3/2O_2$ and forming BaO nanoparticles).

Conclusion

Here, we report on the cycle of morphology changes for BaO/Al_2O_3 NSR catalysts using synchrotron TR-XRD, TEM, and EDS. The results of both TR-XRD and TEM analysis showed that large $Ba(NO_3)_2$ crystallites are formed on the alumina support material during its preparation by an incipient wetness method using an aqueous $Ba(NO_3)_2$ solution. A large fraction of the alumina surface remains Ba-free after this procedure. Upon thermal treatment, these large $Ba(NO_3)_2$ crystallites decompose to form nanosized BaO particles. In fact, we propose that a thin BaO film (monolayer) forms on the alumina support and that the BaO nanoparticles are located on top of this interfacial BaO layer. During room-temperature NO_2 uptake, nanosized (<5 nm) $Ba(NO_3)_2$ particles form, and these particles are stable at room temperature. Heating the material to higher temperature (573 K) in the presence of NO_2 results in the formation of larger $Ba(NO_3)_2$ crystals (~15 nm). At higher temperatures, and even in the absence of NO_2, the average particle size of $Ba(NO_3)_2$ crystallites increases further (~32 nm), and then, as $Ba(NO_3)_2$ decomposes, the nanosized BaO particles reform. In our ongoing research, we are currently investigating the effect of Pt particles on the previously proposed changes in the catalyst morphology during NO_2 uptake and release. We are also investigating the changes in the morphologies of the Ba-containing phases in the NO_x uptake/release processes in the presence of H_2O, CO_x, and hydrocarbons on both BaO/Al_2O_3 and $Pt/BaO/Al_2O_3$ catalysts.

Acknowledgment. Financial support was provided by the U.S. Department of Energy (DOE), Office of Freedom Car and Vehicle Technologies. This work was performed in the Environmental Molecular Sciences Laboratory (EMSL) at the Pacific Northwest National Laboratory (PNNL). The EMSL is a national scientific user facility and supported by the U.S. DOE's Office of Biological and Environmental Research. PNNL is a multi-program national laboratory operated by the U.S. Department of Energy by Battelle Memorial Institute under Contract DE-AC06-76RLO 1830. The work at Brookhaven National Laboratory was financed through Contract DE-AC02-98CH10086 with the DOE (Division of Chemical Sciences).

References and Notes

(1) Miyoshi, N.; Matsumoto, S.; Katoh, K.; Tanaka, T.; Harada, J.; Takahashi, N.; Yokota, K.; Sugiura, M.; Kasahara, K *SEA Paper 950809*, **1995**.
(2) Miyoshi, N.; Matsumoto, S. *Sci. Technol. Catal.* **1998**, 245.
(3) Mahzoul, H.; Brilhac, J. F.; Gilot, P. *Appl. Catal., B* **1999**, *20*, 47.
(4) Anderson, J. A.; Paterson, J. A.; Fernandez-Garcia, M. *Stud. Surf. Sci. Catal.* **2000**, *130*, 1331.
(5) Lietti, L.; Forzatti, P.; Nova, I.; Tronconi, E. *J. Catal.* **2001**, *204*, 175.
(6) Chi, Y.; Chuang, C. S. *J. Phys. Chem. B* **2002**, *104*, 4673.
(7) Prinetto, F.; Ghotti, G.; Nova, I.; Lietti, L.; Tronconi, E.; Forzatti, P. *J. Phys. Chem. B* **2001**, *105*, 12732.
(8) Amberntsson, A.; Persson, H.; Engstrom, P.; Kasemo, B. *Appl. Catal., B* **2002**, *31*, 27.
(9) Westerberg, B.; Fridell, E. *J. Mol. Catal.* **2001**, *165*, 249.
(10) Olsson, L.; Persson, H.; Fridell, E.; Skoglundh, M.; Andersson, B. *J. Phys. Chem. B* **2001**, *105*, 6895.
(11) Schmitz, P. J.; Baird, R. J. *J. Phys. Chem. B* **2002**, *106*, 4172.
(12) Nova, I.; Castoldi, L.; Lietti, L.; Tronconi, E.; Forzatti, P. *Catal. Today* **2002**, *75*, 431.
(13) Prinetto, F.; Ghiotti, G.; Nova, I.; Lietti, L.; Tronconi, I.; Forzatti, P. *Phys. Chem. Chem. Phys.* **2003**, *5*, 4428.
(14) Su, Y.; Amiridis, M. D. *Catal. Today* **2004**, *96*, 31.
(15) Broqvist, P.; Gronbeck, H.; Fridell, E.; Panas, I. *Catal. Today* **2004**, *96*, 71.
(16) Nova, I.; Castoldi, L.; Lietti, L.; Tronconi, E.; Forzatti, P.; Prinetto, F.; Ghiotti, G. *J. Catal.* **2004**, *222*, 377.
(17) Broqvist, P.; Gronbeck, H.; Fridell, E.; Panas, I. *J. Phys. Chem. B* **2004**, *108*, 3523.
(18) Hanson, P. T.; Horton, M. R.; Delgass, N. W.; Lauterbach, J. *Appl. Catal., B* **2003**, *46*, 393.
(19) Szanyi, J.; Kwak, J. H.; Kim, D. H.; Burton, S. H.; Peden, C. H. F. *J. Phys. Chem. B* **2005**, *109*, 27.
(20) Wang, X.; Hanson, J. C.; Frenkel, A. I.; Kim, J.-Y.; Rodriguez, J. A. *J. Phys. Chem. B* **2004**, *108* (36), 13667.
(21) Nowotny, H.; Heger, G. *Acta Chrystallogr. C* **1983**, *39*, 952.
(22) Bensch, W.; Reller, A. *Zeitschrift Kristallogr.* **1986**, *175*, 111.